ornl

OAK RIDGE
NATIONAL
LABORATORY

MARTIN MARIETTA

ORNL/TM-10931

An Investigation of Elastic Guided Waves for Ceramic Joint Evaluation

W. A. Simpson, Jr.
R. W. McClung

OAK RIDGE NATIONAL LABORATORY
CENTRAL RESEARCH LIBRARY
CIRCULATION SECTION
4500N ROOM 175
LIBRARY LOAN COPY
DO NOT TRANSFER TO ANOTHER PERSON
If you wish someone else to see this report, send in name with report and the library will arrange a loan.

OPERATED BY
MARTIN MARIETTA ENERGY SYSTEMS, INC.
FOR THE UNITED STATES
DEPARTMENT OF ENERGY

This report has been reproduced directly from the best available copy.

Available to DOE and DOE contractors from the Office of Scientific and Technical Information, P.O. Box 62, Oak Ridge, TN 37831; prices available from (615) 576-8401, FTS 626-8401.

Available to the public from the National Technical Information Service, U.S. Department of Commerce, 5285 Port Royal Rd., Springfield, VA 22161.
NTIS price codes—Printed Copy: A04 Microfiche A01

This report was prepared as an account of work sponsored by an agency of the United States Government. Neither the United States Government nor any agency thereof, nor any of their employees, makes any warranty, express or implied, or assumes any legal liability or responsibility for the accuracy, completeness, or usefulness of any information, apparatus, product, or process disclosed, or represents that its use would not infringe privately owned rights. Reference herein to any specific commercial product, process, or service by trade name, trademark, manufacturer, or otherwise, does not necessarily constitute or imply its endorsement, recommendation, or favoring by the United States Government or any agency thereof. The views and opinions of authors expressed herein do not necessarily state or reflect those of the United States Government or any agency thereof.

ORNL/TM-10931

Metals and Ceramics Division

AN INVESTIGATION OF ELASTIC GUIDED WAVES FOR CERAMIC JOINT EVALUATION

W. A. Simpson, Jr.
R. W. McClung

Date Published: October 1989

NOTICE: This document contains information of a preliminary nature. It is subject to revision or correction and therefore does not represent a final report.

Prepared for the
DOE Assistant Secretary for Conservation and Renewable Energy,
Office of Energy Utilization Research,
Energy Conversion and Utilization Technologies (ECUT) Program
EG 05 03 00 0

Prepared by the
Oak Ridge National Laboratory
Oak Ridge, Tennessee 37831-6285
operated by
MARTIN MARIETTA ENERGY SYSTEMS, INC.
for the
U.S. DEPARTMENT OF ENERGY
under contract DE-AC05-84OR21400

MARTIN MARIETTA ENERGY SYSTEMS LIBRARIES

3 4456 0328071 3

CONTENTS

	Page
LIST OF FIGURES	v
ABSTRACT	1
INTRODUCTION	1
THEORY	4
CASE 1: RAYLEIGH WAVES	7
CASE 2: "LEAKY" RAYLEIGH WAVES	9
CASE 3: STONELEY WAVES	11
CASE 4: FLUID LAYER	12
CASE 5: THREE-LAYER SOLID	14
NUMERICAL RESULTS	15
CASE 1: RAYLEIGH WAVES	18
CASE 2: "LEAKY" RAYLEIGH WAVES	19
CASE 3: STONELEY WAVES	23
CASE 4: FLUID LAYER	25
CASE 5: THREE-LAYER SOLID	30
BONDING MODEL	34
EXPERIMENT	35
SUMMARY AND CONCLUSIONS	37
ACKNOWLEDGMENTS	38
REFERENCES	39

LIST OF FIGURES

Figure		Page
1	Geometry for a three-layer solid	4
2	Geometry for a semi-infinite layer	8
3	Geometry for a fluid-loaded semi-infinite solid	10
4	Geometry for two solid layers in welded contact	11
5	Geometry for a fluid layer between two solids	13
6	Dispersion curves for guided waves in a fluid layer between quartz	26
7	Dispersion curves for guided waves in the braze layer of a zirconia joint	31
8	Dispersion curves for guided waves in the braze layer of an iron-titanium joint	32
9	Zirconia joint sample for interface wave studies	36
10	Ultrasonic scan of braze joint region	37

AN INVESTIGATION OF ELASTIC GUIDED WAVES FOR CERAMIC JOINT EVALUATION*

W. A. Simpson, Jr., and R. W. McClung

ABSTRACT

The rapid development of ceramic technology has led to the widespread use of ceramics in applications traditionally reserved for metals. Many of these applications, however, require the use of ceramics bonded to other ceramics or to metals in order to achieve the requisite strength. The presence of unbonding in such ceramic joints can now be reliably detected by previously developed ultrasonic techniques, but what is needed is a nondestructive approach which is capable of assessing bond strength directly. A possible tool to achieve this goal is the use of guided elastic waves propagating in the braze layer of a typical ceramic joint.

We describe the theory of guided waves in the center layer of a general three-layer solid. The secular determinant is found, and roots of the secular equation are determined numerically for cases of interest in ceramic joining. Both guided and leaky modes are described, and it is shown that dispersive Stoneley waves can occur for these materials. In addition, the evanescent nature of the guided waves in the bounding solids raises the possiblity of determining the elastic properties of the oxygen depletion layer adjacent to the braze in oxide ceramics. Possible models for incomplete bonding and the effect of this condition on the ultrasonic parameters are also discussed.

INTRODUCTION

The excellent thermal and wear properties of structural ceramics are finding increasing use in applications that have traditionally been reserved for metals. Since many ceramics remain stable at temperatures

*Research sponsored by the U.S. Department of Energy, Office of Energy Utilization Research, under the Energy Conversion and Utilization Technologies (ECUT) Materials Program, under contract DE-AC05-84OR21400 with Martin Marietta Energy Systems, Inc.

well in excess of the melting points of virtually all of the common structural metals, one such application is in high-temperature engines, where the relatively low weight of ceramics provides an additional advantage over such competitors as refractory metals. Unfortunately, with the relatively low fracture toughness and poor machinability of ceramics, practical designs, at least for the near future, will probably consist of ceramic liners attached to metal substrates to combine the wear and thermal properties of ceramics with the strength of metals.

This configuration introduces new problems, however, since one must now guarantee the integrity of the ceramic-to-metal joint as well as that of the component parts themselves. This task is not insurmountable, and techniques have been developed which can detect nondestructively the presence of regions of nonbonding between the ceramic and the metal substrate, even when these regions are as small as 100 μm in diameter.[1] Even for joints which exhibit no demonstrable degree of nonbonding, however, it is well known that failure can still occur, sometimes at stresses well below the expected failure load. This result suggests that, although the component parts are indeed bonded in the sense that local stress is continuous across the interface, the strength of the bond is reduced. One would therefore like to probe the joint region, preferably nondestructively, in a manner such that the local strength of the bond, not just the simple presence or absence of bond, could be assessed. Another aspect of this problem is that the properties of either ceramic or substrate (or both) may vary in the region adjacent to the bond, and the techniques described previously are poorly adapted to the determination of this variation. An example of this behavior is afforded by oxide ceramics, which typically exhibit an oxygen depletion region for $\approx$1 mm from the bond when brazed with certain braze filler metals. The elastic properties in the depletion region are currently inferred by diamond indentation; this technique is clearly destructive.

In considering possible nondestructive techniques to achieve the goals of bond strength determination and assessment of the elastic properties of the materials in and adjacent to the bond, it is clear that conventional elastic bulk waves will be of limited usefulness

because of the very small dimensions of the bond region. The problem of separating the effect of variations in the bulk properties from that of variations in the bond would be virtually insurmountable in this case. However, if one could propagate along the bond layer an elastic wave which was evanescent in the materials on either side of the bond, both goals could be achieved simultaneously. The possibility of generating such waves and the characteristics of the resulting interface propagation are the subjects of this report.

The use of elastic guided waves (waves which are bound to a layer) and interface waves (waves propagating along an interface between media), with a few notable exceptions, has been almost entirely neglected in nondestructive evaluation. One exception, that of waves propagating on the free surface of a solid, was first investigated by Rayleigh.[2] These waves are frequently used for detecting flaws which are surface breaking or which are too near the surface to resolve with bulk waves. A second exception, that of Lamb waves[3] (waves propagating in a plate of thickness comparable to or smaller than a wavelength), has also been used rather widely to monitor changes in the thickness of a plate or to detect the presence of laminar flaws. These two cases represent virtually all of the practical applications of interface waves in nondestructive testing, although many other examples of such waves are known. For example, Love[4] investigated the properties of waves propagating in a layer clad on a semi infinite substrate. Stoneley[5] gave the first comprehensive treatment of waves propagating along the interface between two solids in perfect contact and found that, for a narrow range of material parameters, unattenuated boundary waves may exist. However, this phenomenon has been rarely, if ever, exploited in nondestructive testing, probably because the materials of interest do not satisfy the stringent requirements for such waves. It is shown here that a wave will almost always be present at the interface between any two solids if one permits the wave vector to be complex (i.e., the wave will be attenuated as it propagates along the interface). This type of wave may be more useful than the pure Stoneley wave, but its existence appears not to be widely recognized in nondestructive testing.

In the case of a ceramic joint, we have a general three-layer solid, and it appears that this case has not been examined before in nondestructive testing. This report therefore presents the theory of elastic wave propagation in the braze layer of such a structure, and the solutions to the equations of motion are developed numerically from the theory.

THEORY

Figure 1 shows the geometry of the problem. The interface wave is assumed to have no y dependence and to propagate in the x direction in a braze layer of thickness $2h$. We assume that all materials are linear, homogeneous, and isotropic solids. The equation of motion to be satisfied in each medium is[6]

$$\mu\nabla^2\vec{S} + (\lambda + \mu)\nabla(\nabla\cdot\vec{S}) = \rho\ \partial^2\vec{S}/\partial t^2 \ , \qquad (1)$$

ORNL-DWG 88-13171

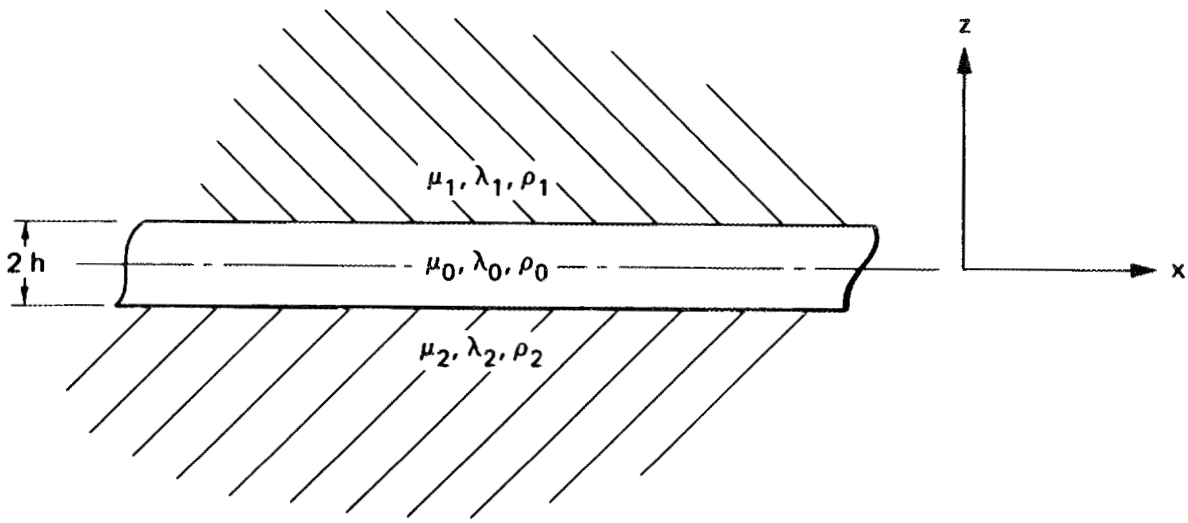

Fig. 1. Geometry for a three-layer solid.

where $\vec{S}$ is the particle displacement, μ and λ are the Lamé elastic constants, and ρ is the density. Now $\vec{S}$ can be defined in terms of the usual potentials:

$$\vec{S} = \nabla\phi + \nabla \times \vec{\psi} \ . \tag{2}$$

The displacement thus contains irrotational and solenoidal components, which give rise to compressional and shear waves, respectively. Substituting Eq. (2) into Eq. (1), we see that ϕ and $\vec{\psi}$ satisfy

$$\nabla^2\phi = (1/C_1^2)\ \partial^2\phi/\partial t^2 \ , \quad \nabla^2\vec{\psi} = (1/C_t^2)\ \partial^2\vec{\psi}/\partial t^2 \ , \tag{3}$$

where C_1 is the longitudinal wave velocity and C_t is the shear wave velocity in the medium in question. We seek solutions whose x dependence is of the form $\exp(ikx)$ and which are independent of y. The latter condition requires that $\vec{\psi} = (0,\ \psi_y,\ 0) = \psi$. We also assume that the solutions are time harmonic of the form $\exp(-i\omega t)$. Thus,

$$\nabla^2\phi = -\omega^2\phi/C_1^2 = -k_1^2\phi \ , \quad \nabla^2\psi = -k_t^2\psi \ , \tag{4}$$

or $(\nabla^2 + k_1^2)\phi = 0$ and $(\nabla^2 + k_t^2)\psi = 0$. Now

$$\nabla^2 = \partial^2/\partial x^2 + \partial^2/\partial z^2 = -k^2 + \partial^2/\partial z^2 \ .$$

Thus, the potentials satisfy

$$d^2\phi/dz^2 = \alpha^2\phi \ , \quad d^2\psi/dz^2 = \beta^2\psi \ , \tag{5}$$

where $\alpha^2 = k^2 - k_1^2$ and $\beta^2 = k^2 - k_t^2$. The solutions to these equations are of the form

$$\phi_m = A_m\exp(\pm\alpha_m z)\exp[i(kx - \omega t)] \ , \quad \psi_m = B_m\exp(\pm\beta_m z)\exp[i(kx - \omega t)] \ ,$$

where the subscript m denotes the region and A_m and B_m are arbitrary coefficients.

The displacement $\vec{S}$ from Eq. (2) is given by

$$S_x = \partial\phi/\partial x - \partial\psi/\partial z \ , \quad S_z = \partial\phi/\partial z + \partial\psi/\partial x \ . \tag{6}$$

The stresses are calculated from the stress-strain relationship in an isotropic solid:

$$\sigma_{ij} = \lambda\delta_{ij}\varepsilon_{kk} + 2\mu\varepsilon_{ij} \ ,$$

where

$$\varepsilon_{ij} = (\partial S_i/\partial x_j + \partial S_j/\partial x_i)/2$$

is the strain tensor and ε_{kk}, the trace of the strain tensor, is the dilatation. The term δ_{ij} is the Kronecker delta function. Substituting for S_k above gives

$$\sigma_{zz} = \lambda(\partial^2\phi/\partial x^2 + \partial^2\phi/\partial z^2) + 2\mu(\partial^2\phi/\partial z^2 + \partial^2\psi/\partial z\partial x)$$

$$= -\lambda k_1^2\phi + 2\mu\alpha^2\phi + 2\mu ik\ \partial\psi/\partial z \ . \tag{7}$$

However, $\alpha^2 = k^2 - k_1^2$; thus,

$$\sigma_{zz} = -(\lambda + 2\mu)k_1^2\phi + 2\mu k^2\phi + 2\mu ik\ \partial\psi/\partial z \ .$$

Also, $(\lambda + 2\mu)k_1^2 = \rho\omega^2 = \mu k_t^2 = \mu(k^2 - \beta^2)$. Therefore,

$$\sigma_{zz}/\mu = (k^2 + \beta^2)\phi + 2ik\ \partial\psi/\partial z \ . \tag{8}$$

Likewise,

$$\sigma_{xz} = \mu(\partial S_x/\partial z + \partial S_z/\partial x) = \mu[2\partial^2\phi/\partial x\partial z - \partial^2\psi/\partial z^2 + \partial^2\psi/\partial x^2] \ ,$$

or

$$\sigma_{xz}/\mu = 2ik\ \partial\phi/\partial z - (k^2 + \beta^2)\psi \ . \tag{9}$$

Now that we have the displacements and stresses in terms of the displacement potentials, the solutions in each region can be written down straightforwardly. Before doing this for the general three-layer solid, however, we shall consider several other examples of interface waves whose solutions are known. This will allow us to compare our numerical results with known or published data. We shall consider five cases, corresponding to increasing order of the secular determinant of the solution: Case 1: Rayleigh waves propagating on the surface of a semi-infinite solid; Case 2: "leaky" Rayleigh waves at a fluid-solid boundary; Case 3: Stoneley waves at the interface between two solids in perfect contact; Case 4: guided waves propagating in a fluid layer between two solids; and Case 5: guided waves propagating in a solid layer between two solids (ceramic joint). Each of these cases was solved numerically by restricting the secular determinant to the appropriate order and finding the roots with a general FORTRAN program to be described later.

CASE 1: RAYLEIGH WAVES

Figure 2 shows the geometry for waves propagating on the surface of a semi-infinite solid. Since there is but a single medium, the displacement potentials are

$$\phi = A \exp(\alpha z) \ , \quad \psi = B \exp(\beta z) \ , \tag{10}$$

where A and B are arbitrary amplitudes to be determined and where $z < 0$, since the solid occupies the lower half space. The common factor $\exp[i(kx - \omega t)]$ has been ignored here and will be omitted for the remainder of this report.

The boundary conditions which must be satisfied are the vanishing of the normal and tangential stresses at the surface of the solid (traction-free surface). Calculating these values from Eqs. (8) and (9), we find that

$$0 = (k^2 + \beta^2)A + 2ik\beta B \ ,$$
$$0 = 2ik\alpha A - (k^2 + \beta^2)B \ . \tag{11}$$

ORNL-DWG 89-2114

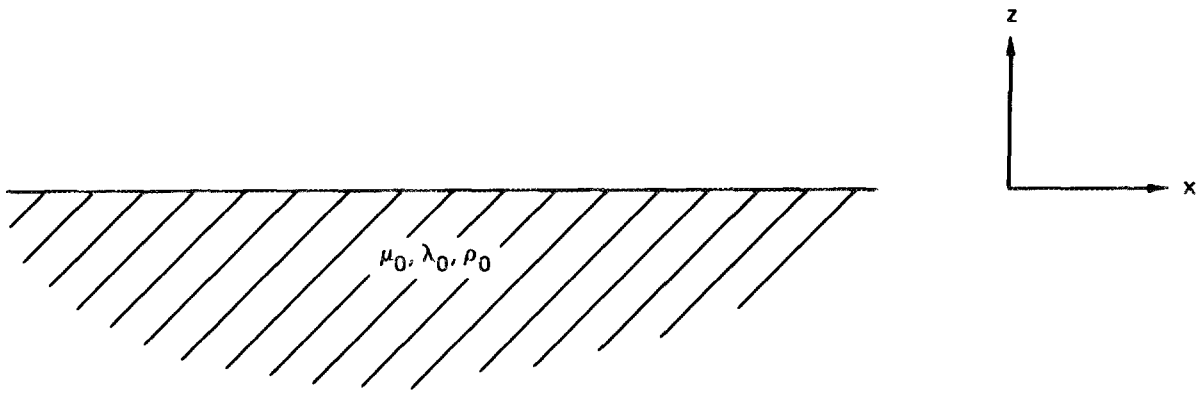

Fig. 2. Geometry for a semi-infinite layer.

If there is to be a nontrivial solution, then

$$\det \begin{pmatrix} (k^2+\beta^2) & 2ik\beta \\ 2ik\alpha & -(k^2+\beta^2) \end{pmatrix} = 0 \ . \tag{12}$$

Solving this secular determinant for k gives the dispersion relation for the waves.

Although we located the roots of the determinant numerically, as must be done in the case of a general solid, for this simple example it is instructive to examine the secular equation analytically for the case of an incompressible solid. Expanding the preceding determinant, we obtain

$$(k^2 + \beta^2)^2 - 4k^2\alpha\beta = 0 \ .$$

If the solid is incompressible, then $\lambda = 0$; thus, $k_1 = 0$ and $\alpha = k$. Then the secular equation becomes

$$(k^2 + \beta^2)^4 = 16k^6\beta^2 = 16k^6(k^2 - k_t^2) \ .$$

Expanding and collecting terms, we obtain

$$k^6 - 3k^4k_t^2/2 + k^2k_t^4/2 - k_t^6/16 = 0 \ .$$

If we let $z = k^2$, the equation becomes

$$z^3 - 3z^2k_t^2/2 + zk_t^4 - k_t^6/16 = 0 \ .$$

This cubic equation can easily be solved by an appropriate substitution.[7] The result is that $C_r = 0.9553C_t$, where C_r is the Rayleigh velocity of the wave.

An analytical solution to the secular equation can also be found for the Poisson relation (i.e., when $\lambda = \mu$). In this case, $C_r = 0.9194C_t$. Thus, for virtually all solids, the Rayleigh velocity will range from $0.90C_t$ to $0.95C_t$. If an exact value is required for an arbitrary solid, the secular determinant must be solved numerically. This is our approach, and the value obtained for Rayleigh waves propagating on the surface of iron is given in the section on "Numerical Results."

The roots found previously were all real and smaller in magnitude than C_t. Since $\beta = (k^2 - k_t^2)^{1/2}$, we see that β is real, and thus the wave is exponentially damped with depth in the solid. The wave is therefore bound to the surface and propagates along the interface without loss.

CASE 2: "LEAKY" RAYLEIGH WAVES

If, instead of vacuum above the semi-infinite solid treated in Case 1, we substitute a fluid (see Fig. 3), the boundary conditions are altered and additional waves may be present. The change in boundary

ORNL-DWG 89-2115

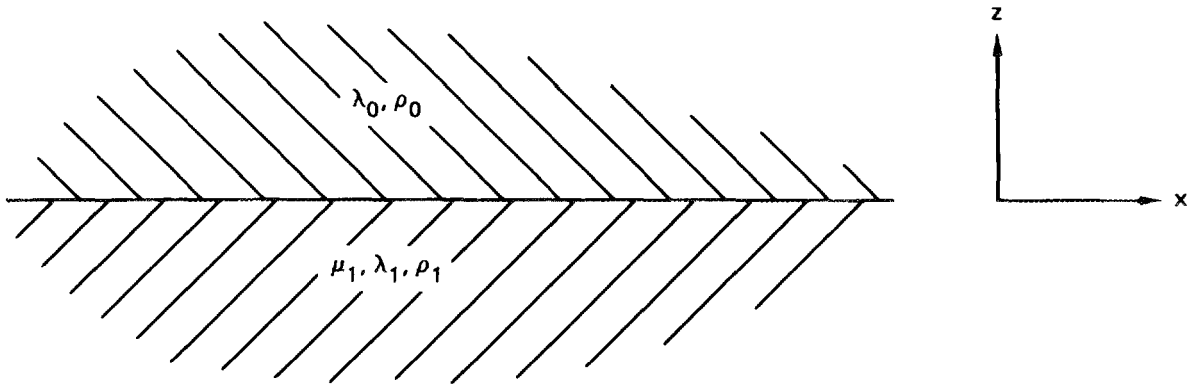

Fig. 3. Geometry for a fluid-loaded semi-infinite solid.

conditions reflects the fact that a propagating (nonattenuating) wave may be present in the fluid, whereas this is, of course, impossible in the case of vacuum. The existence of this wave in the fluid, which is continuously radiated by the surface wave as it propagates along the boundary, means that the interface wave is damped (i.e., the wave vector k is complex). Such a condition, in which an interface wave "leaks" energy into the bounding materials, is called a "leaky" wave.

To learn the characteristics of the leaky wave, we assume the fluid to be perfect ($\mu = 0$) and write the displacement potentials in each region:

$$\begin{aligned} \phi_1 &= A_1 \exp(-\alpha_1 z) \ , \\ \psi_1 &= 0 \ , \end{aligned} \qquad z > 0 \ , \qquad \begin{aligned} \phi_2 &= A_2 \exp(\alpha_2 z) \ , \\ \psi_2 &= B_2 \exp(\beta_2 z) \ , \end{aligned} \qquad z < 0 \ . \tag{13}$$

The boundary conditions at the fluid–solid interface are the continuity of normal displacement and normal and tangential stress (actually, the

tangential stress must vanish since the fluid cannot support a shear wave). Substituting the potentials of Eq. (13) into the expression for S_z in Eq. (6) and using Eqs. (8) and (9) for the stresses [the first term in Eq. (7), $-\lambda k_1^2\phi$, is used for the stress in the fluid since $\mu = 0$ there], we obtain the secular determinant for leaky Rayleigh waves:

$$\det \begin{bmatrix} -\alpha_1 & -\alpha_2 & -ik \\ -\lambda k_1^2 & -\mu_2(k^2+\beta^2) & -2ik\mu_2\beta_2 \\ 0 & -2ik\alpha_2 & \mu_2(k^2+\beta^2) \end{bmatrix} = 0. \qquad (14)$$

A complex root, corresponding to a damped interface wave, was found for this determinant and is discussed later.

CASE 3: STONELEY WAVES

We now substitute a solid for the upper medium, as shown in Fig. 4. In this case, both the normal and the tangential components of displacement and stress are continuous across the interface. Since both

ORNL-DWG 89-2116

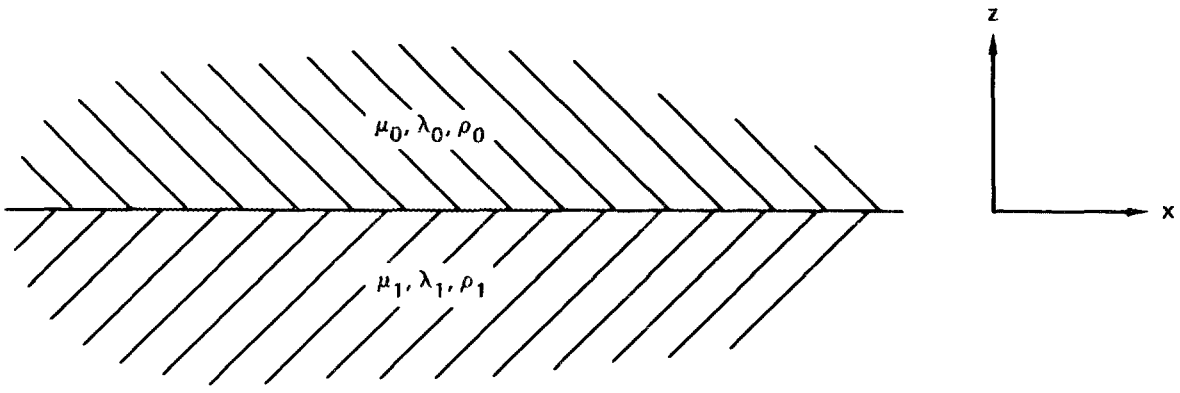

Fig. 4. Geometry for two solid layers in welded contact.

boundary materials are solids, potentials are required for shear waves as well as compressional waves in each medium. The potentials in each region are

$$\begin{aligned} \phi_1 &= A_1 \exp(-\alpha_1 z) \ , \\ \psi_1 &= B_1 \exp(-\beta_1 z) \ , \end{aligned} \qquad z > 0 \ , \qquad (15)$$

$$\begin{aligned} \phi_2 &= A_2 \exp(\alpha_2 z) \ , \\ \psi_2 &= B_2 \exp(\beta_2 z) \ , \end{aligned} \qquad z < 0 \ .$$

Substituting these potentials into Eqs. (6), (8), and (9) leads to the determinantal equation

$$\det \begin{pmatrix} -\alpha_1 & ik & -\alpha_2 & -ik \\ ik & \beta_1 & -ik & \beta_2 \\ \mu_1(k^2+\beta_1^2) & -2ik\mu_1\beta_1 & -\mu_2(k^2+\beta_2^2) & -2ik\mu_2\beta_2 \\ -2ik\mu_1\alpha_1 & -\mu_1(k^2+\beta_1^2) & -2ik\mu_2\alpha_2 & \mu_2(k^2+\beta_2^2) \end{pmatrix} = 0 \ . \quad (16)$$

Stoneley[5] was able to solve this determinant for real roots and found that undamped interface waves could exist between two solids only for a very narrow range of material parameters. However, we shall later see that a far richer ensemble of waves can exist if we admit complex values for the wave vector k.

CASE 4: FLUID LAYER

Figure 5 shows the geometry for a fluid layer between two solids. We assume that the center of the layer corresponds to $z = 0$ and that the layer half thickness is h. Since the layer is of finite thickness, the solutions for waves in the layer are given by functions of the form $\exp(\pm\alpha z)$. We shall write the potential ϕ_0 in the layer as

$$\phi_0 = A_0 \cos(\alpha_0 z) + B_0 \sin(\alpha_0 z) \ .$$

ORNL-DWG 89-2117

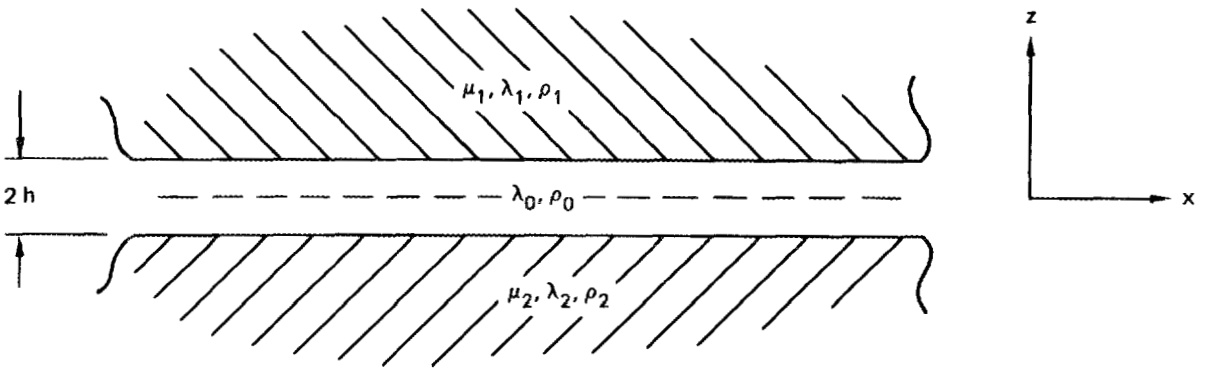

Fig. 5. Geometry for a fluid layer between two solids.

The solutions will thus exhibit symmetric ($B_0 = 0$) or antisymmetric ($A_0 = 0$) behavior with respect to the centerline $z = 0$. With this choice of potentials, however, the terms containing $(k^2 + \beta_0^2)$ in Eqs. (8) and (9) must be replaced by $(k^2 - \beta_0^2)$. Since the layer thickness is finite, we shall also see that the admissible waves are dispersive, in contrast with the previous examples of interface waves.

The potentials in each region are given by

$$\begin{aligned}
\phi_1 &= A_1 \exp(-\alpha_1 z) \ , \\
\psi_1 &= B_1 \exp(-\beta_1 z) \ , \qquad z > h \ , \\
\phi_0 &= A_0 \cos(\alpha_0 z) + B_0 \sin(\alpha_0 z) \ , \qquad |z| < h \ , \\
\phi_2 &= A_2 \exp(\alpha_2 z) \ , \\
\psi_2 &= B_2 \exp(\beta_2 z) \ , \qquad z < -h \ .
\end{aligned} \tag{17}$$

The boundary conditions to be satisfied at $z = \pm h$ are the continuity of the normal displacements and the normal and tangential stresses. Substituting these potentials into Eqs. (8)–(10) [and using Eq. (7) with $\mu = 0$ for the stress in the fluid layer], we obtain the determinantal equation for waves in the fluid layer:

$$\det\begin{bmatrix} -\alpha_1 e^{-\alpha_1 h} & ike^{-\beta_1 h} & \alpha_0 \sin \alpha_0 h & -\alpha_0 \cos \alpha_0 h & 0 & 0 \\ \mu_1(k^2+\beta_1^2)e^{-\alpha_1 h} & -2ik\mu_1\beta_1 e^{-\beta_1 h} & \lambda k_0^2 \cos \alpha_0 h & \lambda k_0^2 \sin \alpha_0 h & 0 & 0 \\ 2ik\mu_1\alpha_1 e^{-\alpha_1 h} & \mu_1(k^2+\beta_1^2)e^{-\beta_1 h} & 0 & 0 & 0 & 0 \\ 0 & 0 & \alpha_0 \sin \alpha_0 h & \alpha_0 \cos \alpha_0 h & -\alpha_2 e^{-\alpha_2 h} & -ike^{-\beta_2 h} \\ 0 & 0 & -\lambda k_0^2 \cos \alpha_0 h & \lambda k_0^2 \sin \alpha_0 h & -\mu_2(k^2+\beta_2^2)e^{-\alpha_2 h} & -2ik\mu_2\beta_2 e^{-\beta_2 h} \\ 0 & 0 & 0 & 0 & -2ik\mu_2\alpha_2 e^{-\alpha_2 h} & \mu_2(k^2+\beta_2^2)e^{-\beta_2 h} \end{bmatrix} = 0 \ . \qquad (18)$$

There are several characteristics of the wave propagation which can be predicted from the form of the preceding determinant. First, for identical solids on either side of the fluid layer, the symmetry of the secular determinant about the plane $z = 0$ allows the determinantal equation to be factored, indicating that two classes of waves will be present.[8] Second, as the layer thickness goes to zero, the determinant reduces to that for two solids in slip (frictionless) contact; thus, we expect the zero-thickness wave propagation to reduce to that of a Rayleigh wave at the boundary. The dispersion curves for the fluid layer problem are presented later.

CASE 5: THREE-LAYER SOLID

For the three-layer solid (Fig. 1), both longitudinal and shear waves can exist in the center layer, and thus six potentials are required. The potentials in each region are

$$\begin{aligned} \phi_1 &= A_1 \exp(-\alpha_1 z) \ , \\ \psi_1 &= B_1 \exp(-\beta_1 z) \ , \end{aligned} \qquad z > h \ ,$$

$$\begin{aligned} \phi_0 &= A_0 \cos(\alpha_0 z) + B_0 \sin(\alpha_0 z) \ , \\ \psi_0 &= C_0 \cos(\beta_0 z) + D_0 \sin(\beta_0 z) \ , \end{aligned} \qquad |z| < h \ , \qquad (19)$$

$$\begin{aligned} \phi_2 &= A_2 \exp(\alpha_2 z) \ , \\ \psi_2 &= B_2 \exp(\beta_2 z) \ . \end{aligned} \qquad z < -h$$

The boundary conditions are that both the normal and the tangential displacements and stresses must be continuous at $\pm h$. As in the last

example, the choice of trigonometric functions for the potentials in the braze layer requires that the expressions for the stresses, Eqs. (8) and (9), be modified by replacing the term $(k^2 + \beta_0^2)$ by $(k^2 - \beta_0^2)$. The secular determinant for this problem is given in Eq. (20).

As in the case of the fluid layer, the form of the determinant suggests that, for identical solids on either side of the central layer, symmetry about $z = 0$ can again be invoked to show that the secular determinant may be factored into two terms. Also, the determinant reduces to that for two solids in perfect contact when the layer thickness goes to zero. Hence, we expect that the zero-thickness solution will be a Stoneley wave and that the solution in this limit will reduce to an ordinary shear wave when the solids are identical.

For the three-layer solid problem, the secular determinant becomes:

$$\det \begin{vmatrix} -\alpha_1 e^{-\alpha_1 h} & ike^{-\beta_1 h} & \alpha_0 \sin \alpha_0 h & -\alpha_0 \cos \alpha_0 h & -ik \cos \beta_0 h & -ik \sin \beta_0 h & 0 & 0 \\ ike^{-\alpha_1 h} & \beta_1 e^{-\beta_1 h} & -ik \cos \alpha_0 h & -ik \sin \alpha_0 h & -\beta_0 \sin \beta_0 h & \beta_0 \cos \beta_0 h & 0 & 0 \\ \mu_1(k^2+\beta_1^2)e^{-\alpha_1 h} & -2ik\mu_1\beta_1 e^{-\beta_1 h} & -\mu_0(k^2-\beta_0^2) \cos \alpha_0 h & -\mu_0(k^2-\beta_0^2) \sin \alpha_0 h & 2ik\mu_0\beta_0 \sin \beta_0 h & -2ik\mu_0\beta_0 \cos \beta_0 h & 0 & 0 \\ -2ik\mu_1\alpha_1 e^{-\alpha_1 h} & -\mu_1(k^2+\beta_1^2)e^{-\beta_1 h} & 2ik\mu_0\alpha_0 \sin \alpha_0 h & -2ik\mu_0\alpha_0 \cos \alpha_0 h & \mu_0(k^2-\beta_0^2) \cos \beta_0 h & \mu_0(k^2\beta_0^2) \sin \beta_0 h & 0 & 0 \\ 0 & 0 & \alpha_0 \sin \alpha_0 h & \alpha_0 \cos \alpha_0 h & ik \cos \beta_0 h & -ik \sin \beta_0 h & -\alpha_2 e^{-\alpha_2 h} & -ike^{-\beta_2 h} \\ 0 & 0 & ik \cos \alpha_0 h & -ik \sin \alpha_0 h & -\beta_0 \sin \beta_0 h & -\beta_0 \cos \beta_0 h & -ike^{-\alpha_2 h} & \beta_2 e^{-\beta_2 h} \\ 0 & 0 & \mu_0(k^2-\beta_0^2) \cos \alpha_0 h & -\mu_0(k^2-\beta_0^2) \sin \alpha_0 h & 2ik\mu_0\beta_0 \sin \beta_0 h & 2ik\mu_0\beta_0 \cos \beta_0 h & -\mu_2(k^2+\beta_2^2)e^{-\alpha_2 h} & -2ik\mu_2\beta_2 e^{-\beta_2 h} \\ 0 & 0 & 2ik\mu_0\alpha_0 \sin \alpha_0 h & 2ik\mu_0\alpha_0 \cos \alpha_0 h & -\mu_0(k^2-\beta_0^2) \cos \beta_0 h & \mu_0(k^2-\beta_0^2 \sin \beta_0 h & -2ik\mu_2\alpha_2 e^{-\alpha_2 h} & \mu_2(k^2+\beta_2^2)e^{-\beta_2 h} \end{vmatrix} = 0 \ . \quad (20)$$

NUMERICAL RESULTS

As mentioned previously, we have chosen to solve the secular equations numerically. This was not a particularly difficult decision

in light of the fact that the equations appear to be intractable to analytical approaches except for a very few specific cases or unless we make some simplifying assumptions. Since we wanted to ensure a solution for all choices of material parameters, we wrote a general FORTRAN program to locate all roots of each secular determinant.

A few comments regarding the existence and nature of roots are in order here. Since the secular determinant for each problem leads to an nth-order equation for the wave vector, k, of the interface or guided wave, there will always be n roots. Some (or all) of these roots may be complex, and there may be multiple real roots. The complex roots indicate that the wave is damped, since $\exp(ikx) = \exp(-k_i x)\exp(ik_r x)$, where k_r and k_i are the real and imaginary parts of the wave vector, respectively. Some of the roots may not correspond to physical waves [e.g., those complex roots for which $k_i < 0$ (which corresponds to an exponentially growing wave)], and those which are acceptable may not be practical because they are damped too rapidly. In all cases, however, there will be n roots, some of which will probably correspond to a physically realizable interface or guided wave. Thus, although the identification of real roots of the solid-solid secular determinant with Stoneley waves is appropriate, in nondestructive evaluation the fact that no real roots exist is sometimes interpreted to mean that no interface wave exists, which is incorrect. The complicated nature of these roots, including the previous incorrect identification of the limiting cases of some of the roots, has been pointed out by Pilant.[9]

In locating the roots of the secular equation, we note that there is a branch point associated with each square root which defines the wave vectors α and β [see Eq. (5)]. Thus, the roots of the secular equation will lie on several Riemann sheets. In defining the potentials as we have in Eqs. (10), (13), (15), (17), and (19), however, we see that the real roots (corresponding to waves evanescent in the surrounding solids) should lie on the sheet corresponding to all positive branches of the square root functions. In addition, leaky modes (if present) should occur on the sheet corresponding to the negative branch of the wave vector for the potential ψ in the medium in which the leaky wave propagates. We emphasize that, except for the case

of Stoneley waves, we did not search each Riemann sheet for all possible roots, although this could certainly be done. Hence, there may be modes other than those we report. We believe that the physically significant waves can be found by application of the preceding principles, however.

We tried a number of different approaches in locating the roots of the secular determinant. In the end, however, we settled on a technique in which we first search the complex phase velocity plane for local minima of the |det| function, using a relatively coarse step along both real and imaginary axes. The step size must be chosen carefully since too coarse a step may miss a root while too fine a step requires excessive computer time. Each minimum is then located precisely by using a two-variable Newton's approximation method; that is, the slope of the surface in both the real and the imaginary direction is calculated by using a step size of 10^{-10}, and a weighted average is then taken to yield a conservative estimate of the location of the minimum. We found that a rather arcane collection of test statements was necessary to guarantee convergence to the minimum and to prevent the program from falling into an endless cycle of corrections which overshoot the minimum or approach too slowly. In the final version, the program will generally locate the minimum of the surface within 10^{-8} along both real and imaginary axes within ten steps (often within five steps, depending on the local nature of the surface). A final test determines if the minimum corresponds to a true root or merely to a nonzero minimum (which occurs, for example, when either the real or the imaginary part of the determinant, but not both, goes through zero).

The main routine of the FORTRAN program permits secular determinants up to 16×16 to be solved (this size can easily be expanded if needed). The program need be compiled only once and is then linked with a subroutine called MATRIX, which defines the elements of the determinant. Thus, the main program must be relinked for each new determinant (but not for each change of materials for a given order of determinant, since this information is input to the main program and passed to MATRIX).

The determinant is calculated by a subroutine which uses Gaussian elimination with partial pivoting. The running time for the program on

the 8 × 8 determinant is only a few minutes on an IBM PC-AT (8 MHz with 12 MHz accelerator card) to cover the range $0 < C_r < 4$ and $-0.3 < C_i < 0$, where C_r and C_i are the real and imaginary parts of the phase velocity, respectively.

After the roots of the secular equation have been found, one would also like to know the amplitudes of the various waves (i.e., the coefficients A_m and B_m for each potential, as well as the wave vectors α_m and β_m). The wave vectors are computed from the definitions [Eq. (5)] and printed for each root. The coefficients are determined by solving the homogeneous matrix equation

$$\tilde{D}\tilde{Y} = 0 \ , \tag{21}$$

where $\tilde{D}$ is the determinant matrix and $\tilde{Y}$ is the coefficient matrix. Since the equation is homogeneous, one can only solve for ratios of coefficients. Thus, we set one of the coefficients to 1 and solve for the others in terms of the prescribed amplitude. For guided waves (e.g., Case 4 and Case 5 presented earlier), which generally exhibit symmetric and antisymmetric properties, the program will automatically determine which type of symmetry is appropriate to the root in question and solve for all other coefficients in terms of the coefficient of the symmetric or antisymmetric term. This is done by first assuming that the mode is symmetric (coefficient = 1) and solving for the antisymmetric coefficient. If the absolute value of the result is > 1, then the solution is repeated with the antisymmetric coefficient set to 1. For pure modes, this approach will yield a coefficient of very nearly zero for the opposite symmetry.

For interface waves (no finite layers), the program arbitrarily sets the coefficient of the potential ψ in the upper medium to unity. All coefficients are then printed in the analysis of each root.

CASE 1: RAYLEIGH WAVES

The secular determinant for Rayleigh waves was given by Eq. (12). The material chosen was iron, for which the properties are $\rho = 7.86$ g/cm^3,

C_l = 5.89 km/s, and C_t = 3.21 km/s. Since the FORTRAN program was written for the general case of dispersive interface waves, an input frequency range must be specified, even though there is no dispersion for Rayleigh waves. In the present case, 1 MHz was entered for both upper and lower frequencies. Since Rayleigh waves correspond to real roots of the secular determinant, the imaginary axis search range was set to zero. The real axis velocity search range was specified as 0 to 4 km/s. The program found a single root at

$$C = 2.97132 + i\ 0.00000 \text{ km/s} ,$$

where C is the phase velocity of the Rayleigh wave. This value is $0.9256C_t$, which is in the estimated range from $0.90C_t$ to $0.95C_t$ mentioned earlier.

The wave vectors for this case are

$$\alpha = 1.82582 + i\ 0.00000 ,$$

$$\beta = 0.80015 + i\ 0.00000 .$$

Since $z < 0$ in this medium, we see that both potentials are evanescent in the iron.

CASE 2: "LEAKY" RAYLEIGH WAVES

The determinant for leaky Rayleigh waves is given by Eq. (14). We assume that the solid is iron and the fluid layer is water. The salient material properties of water are ρ = 1 g/cm^3 and C_l = 1.483 km/s. The imaginary axis search range was from −0.3 to 0 km/s, and the real axis range was from 0 to 4 km/s. We specified the Riemann sheet for the search to be the negative branch for α_l and the positive branch for the other wave vectors. Since there is again no dispersion, the frequency was specified to be 1 MHz. The program found a single root on this sheet at

$$C = 2.97255 - i\ 3.17361 \times 10^{-2} \text{ km/s} .$$

The phase velocity for the leaky wave is thus slightly higher than that of the Rayleigh wave. Since C is complex, we see that the wave is damped. This is best seen by noting that $k = \omega/C$. Thus

$$k = 2.11349 + i\ 2.25645 \times 10^{-2}\ \mathrm{mm}^{-1}$$

at 1 MHz. Therefore,

$$\exp(ikx) = \exp[(-2.25645 \times 10^{-2})x]\exp[i(2.11349x)] \ .$$

The wave is thus attenuated by 2.25645×10^{-2} neper/mm, or about 0.2 db/mm, as it propagates along the interface.

The values for the other wave vectors yield some very interesting results for this problem. These values are

$$\alpha_1 = -1.29870 \times 10^{-2} - i\ 3.67311\ \mathrm{mm}^{-1} \ ,$$

$$\alpha_2 = 1.82457 + i\ 2.61375 \times 10^{-2}\ \mathrm{mm}^{-1} \ ,$$

$$\beta_2 = 0.79911 + i\ 5.96788 \times 10^{-2}\ \mathrm{mm}^{-1} \ .$$

The potentials in the iron all yield damped waves as before. The value for α_1 requires further explanation, however.

Since we specified the negative branch for α_1, both real and imaginary parts are less than zero. Equation (13), however, requires that $\phi_1 = A_1\exp(-\alpha_1 z)$. Substituting the value determined by the computer program yields

$$\phi_1 = A_1\exp[(1.29870 \times 10^{-2})z]\exp[i(3.67311z)] \ .$$

The result seems to imply that the wave grows exponentially with distance from the interface. The discrepancy results from the fact that, as stated previously, the common factor $\exp[i(kx - \omega t)]$ has been dropped from all the potentials. Thus, Eq. (13) should state:

$$\phi_1 = A_1\exp(-\alpha_1 z)\exp[i(kx - \omega t)] \ .$$

The factor $\exp(-i\omega t)$ is not important here and may be dropped. Substituting the value for k obtained previously, we obtain

$$\phi_1 = A_1 \exp[(1.29870 \times 10^{-2})z]\exp[(-2.25645 \times 10^{-2})x]$$
$$\times \exp[i(2.11349x + 3.67311z)] \ .$$

The complex exponential defines a direction of propagation in the water which makes an angle of 60°.084 with respect to the interface (or 29°.916 with respect to the normal to the interface). Along this line of propagation, the two real exponentials are exactly equal and opposite and therefore cancel. Thus, the wave defined by the potential ϕ_1 is a real (undamped) wave propagating in the water at an angle of 29°.916 with respect to the normal to the interface. This is the leaky wave, which is radiated by the interface wave as it propagates along the boundary of the solid and which is responsible for the damping of the interface wave. Thus, the wave vector of the leaky wave potential must be complex with negative real and imaginary parts. This is the reason for our earlier statement that the leaky waves should be found on the negative branch of the wave vector for the potential in the medium in which the leaky wave propagates.

The apparent exponential growth of the leaky wave can also be explained in another way. If we fix the value of the x-coordinate (i.e., if we consider a fixed point on the interface), and if we then examine the behavior of the leaky wave as z increases, we shall indeed find that the amplitude increases with distance from the interface, since we will be intercepting rays which have come from earlier points on the boundary where the interface wave is less highly damped. Along the direction of propagation of the leaky wave, however, the amplitude is constant.

Since the interface wave radiates a bulk wave into the water, the inverse situation (i.e., a bulk wave incident on the interface at the critical angle generates the interface wave) is also possible. This is a much more useful configuration for nondestructive evaluation because the leaky interface wave can be generated by a conventional angle-beam

immersion ultrasonic system whereas the undamped interface wave requires special contact transducer wedges for each material to be examined. For the leaky wave case, it is instructive to calculate the critical angle. This was obtained earlier from the real part of k and the imaginary part of α_1. It should also be derivable from the bulk and interface wave velocities and Snell's law. If we use the bulk wave velocity of 1.483 km/s and the real part of the interface wave velocity given previously, however, the results do not agree; they are close only because the imaginary part of k is small compared with the real part (i.e., the damping is small). Using the absolute value of the interface wave velocity does not correct the problem. To see where the problem arises, we write Snell's law in the form

$$k_0 \sin \theta = k \ , \tag{22}$$

where k_0 is the wave vector of the incident bulk wave, k is the wave vector of the interface wave, and θ is the angle of incidence for the interface wave. Now k_0 is real, while k is complex. Hence, θ must be complex. The critical angle corresponds to the real part of the complex angle of incidence, which can be found as follows. The sine of the incident angle may be expanded to yield

$$\sin \theta = \sin \theta_r \cosh \theta_i + i \cos \theta_r \sinh \theta_i \ , \tag{23}$$

where θ_r and θ_i are the real and imaginary parts of the complex angle of incidence. Likewise,

$$\cos \theta = \cos \theta_r \cosh \theta_i - i \sin \theta_r \sinh \theta_i \ . \tag{24}$$

From Eq. (22),

$$\sin \theta = (k_r/k_0) + i \ (k_i/k_0) \ .$$

Thus, from Eq. (23),

$$\sin \theta_r \cosh \theta_i = k_r/k_0 \ , \quad \cos \theta_r \sinh \theta_i = k_i/k_0 \ .$$

Now cos θ can be calculated from

$$\cos\theta = (1 - \sin^2\theta)^{1/2} ,$$

and the real and imaginary parts can be equated to the corresponding terms in Eq. (24). Comparing Eqs. (23) and (24), we see that

$$\mathrm{Re}(\sin\theta)/\mathrm{Re}(\cos\theta) = \tan\theta_r .$$

When this is done for the above example, we find that the angle obtained is precisely that computed earlier from k_r and the imaginary part of α_1.

The calculations just demonstrated would never actually be performed in practice since the critical angle is readily available from the computer output. The result establishes that the same value can be obtained from the two velocities and Snell's law, however, a fact which is not apparent from the computer results. In addition, it appears possible that for some problems $\mathrm{Re}(k)/k_0 > 1$, and thus failure to recognize that θ is complex will lead to values of sin θ that exceed 1.

CASE 3: STONELEY WAVES

The secular determinant for this case is given in Eq. (16). Several different material combinations were treated by Lee and Corbly,[10] and we chose those examples to test our program. We began with the case of titanium bonded to iron since this case is known to support a Stoneley wave. The properties of iron have already been given, and those of titanium are $\rho = 4.44$ g/cm^3, $C_1 = 6.11$ km/s, and $C_t = 3.27$ km/s. We first searched for roots along the real velocity axis since any such roots will be the true Stoneley waves. The frequency was 1 MHz, although this is unimportant since the waves are not dispersive. The program found a single root at

$$C = 3.20865 + i\ 0.00000 \text{ km/s} .$$

The value given in ref. 9 was 3.209 km/s. All wave vectors were pure real, indicating an undamped interface wave that is evanescent in both the iron and the titanium.

We next selected the case of aluminum bonded to iron. The properties of aluminum are $\rho = 2.77$ g/cm^3, $C_l = 6.31$ km/s, and $C_t = 3.10$ km/s. No true Stoneley wave exists for these materials, and this was confirmed by our program, which found no roots on the real axis in the range $0 < C < 6$ km/s. We next specified that the Riemann sheet corresponding to the negative branch of β_1 and the positive branches of all other wave vectors be searched. The real axis range was $0 < C_r < 6$ km/s, and the imaginary axis range was $-0.3 < C_i < 0$. The program found a root at

$$C = 3.14829 - i\ 7.24406 \times 10^{-3}\ \text{km/s}\ .$$

The value given in ref. 10 was $3.1483 - i\ 0.00724$ km/s. The wave vectors for this case were

$$\alpha_1 = 1.72958 + i\ 5.29875 \times 10^{-3}\ \text{mm}^{-1}\ ,$$

$$\beta_1 = -2.58410 \times 10^{-2} - i\ 0.354654\ \text{mm}^{-1}\ ,$$

$$\alpha_2 = 1.68672 + i\ 5.43341 \times 10^{-3}\ \text{mm}^{-1}\ ,$$

$$\beta_2 = 0.390083 + i\ 2.34940 \times 10^{-2}\ \text{mm}^{-1}\ .$$

As before, α_1, α_2, and β_2 lead to damped potentials. The wave vector β_1 corresponds to a leaky wave, however. From the imaginary part of β_1 and the preceding phase velocity, we see that the wave is propagating upward in the aluminum at an angle of 79°.9 with respect to the normal to the interface and is a shear wave. Thus, the leaky Stoneley wave can be excited by a shear wave in the aluminum incident on the interface at an angle of 79°.9.

The next case considered was aluminum bonded to titanium, which is also discussed in ref. 10. The program found a single leaky wave on the same Riemann sheet as that for aluminum bonded to iron. The phase velocity is

$$C = 3.25449 - i\ 2.49132 \times 10^{-2}\ \text{km/s}\ .$$

The value given in ref. 10 is 3.2545 − i 0.025 km/s. The wave vectors of the potentials are

$$\alpha_1 = 1.65391 + i\ 1.72495 \times 10^{-2}\ \text{mm}^{-1}\ ,$$

$$\beta_1 = -4.60666 \times 10^{-2} - i\ 0.619302\ \text{mm}^{-1}\ ,$$

$$\alpha_2 = 1.63385 + i\ 1.74614 \times 10^{-2}\ \text{mm}^{-1}\ ,$$

$$\beta_2 = 0.225124 + i\ 0.126727\ \text{mm}^{-1}\ .$$

From these values and the preceding phase velocity, the wave is found to be propagating in the aluminum at an angle of 72°.2 with respect to the normal to the interface.

A more stringent test of our computer program was afforded by the results of Pilant,[9] who showed that there were 16 roots to the Stoneley equation and who found all of these roots numerically for a number of material combinations. Pilant's analysis assumed materials for which $(C_t/C_1)^2 = 1/3$. The behavior of the roots was then studied as the ratios $(C_{t2}/C_{t1})^2$ and (ρ_1/ρ_2) varied. We repeated this study for the case $(C_{t2}/C_{t1})^2 = 0.8$ and $(\rho_1/\rho_2) = 0.5$. Two hypothetical solids were assumed with the following material parameters: $\rho_1 = 1.5$ g/cm^3, $C_{11} = 5.19615$ km/s, $C_{t1} = 3$ km/s, $\rho_2 = 3$ g/cm^3, $C_{12} = 4.64758$ km/s, and $C_{t2} = 2.68328$ km/s. The range for the search was $0 < C_r < 7$ and $-0.4 < C_i < 0$. Our program easily found all 16 roots, and they were the same as those found by Pilant. [Since complex roots with positive imaginary parts are physically untenable, we searched only the negative imaginary half plane, finding 12 roots (8 real and 4 complex). The other 4 roots are presumably positive and were not given by Pilant.]

CASE 4: FLUID LAYER

The secular determinant for a fluid layer between two solids is given by Eq. (18). This problem was also studied by Staecker and Wang.[8]

Since we have a layer of finite thickness, we should expect the guided waves to exhibit dispersion, and this is found to be the case.

The case chosen was that of a water layer between two fused quartz half spaces. The properties of the quartz are $\rho = 2.6$ g/cm^3, $C_l = 5.57$ km/s, and $C_t = 3.51$ km/s. We first considered only pure guided waves (no damping) by searching along the real axis for roots of the secular equation. Since dispersion is present, the calculations were performed for a range of frequencies. The results are best interpreted by normalizing the velocities and layer thickness; thus, the roots (velocities) were divided by the velocity of sound in water, and the layer thickness was divided by the wavelength of sound in water at the specified frequency. Figure 6 shows the results. The permissible waves are seen to consist of a number of symmetric or antisymmetric modes. This figure should be compared with Figs. 2*a* and 2*b* of ref. 8, where the slight differences are presumably due to differences in material parameters, which were not described in the reference.

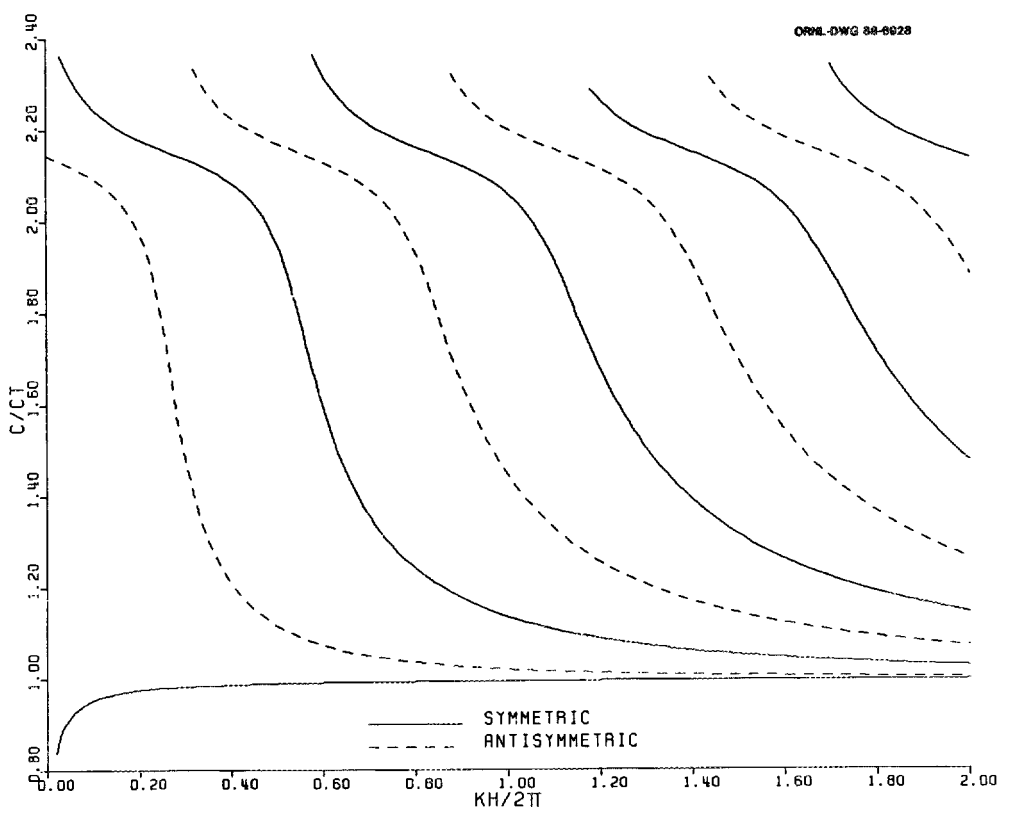

Fig. 6. Dispersion curves for guided waves in a fluid layer between quartz.

In the limit as the frequency (or the thickness of the fluid layer) goes to infinity, the phase velocity of each mode approaches that of an ordinary wave in the fluid. This is to be expected since the propagation approaches that of an ordinary bulk wave in fluid when the normalized layer thickness becomes large. As the normalized layer thickness approaches zero, however, Fig. 6 shows that all of the waves vanish but one, the lowest-order antisymmetric mode. The phase velocity of this wave in the limit is just that of a Rayleigh wave propagating along the surface of the quartz. The lowest-order antisymmetric mode is thus a dispersive Rayleigh wave.

The behavior of the "slow wave" (i.e., the lowest-order symmetric mode, whose phase velocity is less than that of the normal wave in the fluid) is also correctly described by our results. Reference 8 indicates that, for this wave, the amplitudes will be hyperbolic rather than sinusoidal as assumed in Eq. (17). This was confirmed by our program, where α_0 was found to be pure imaginary, and the sine or cosine of a pure imaginary argument becomes the hyperbolic sine or cosine of the same pure real argument. For all other modes α_0 was pure real.

The group velocity of a given wave, which has not been mentioned previously since dispersion was not present, can be obtained from the data in Fig. 6. By definition, the group velocity V_g is given by

$$V_g = d\omega/dk \ .$$

But $\omega = Ck$, where C is the phase velocity. Thus

$$V_g = C + k(dC/dk) \ . \tag{25}$$

The term dC/dk is proportional to the slope of the phase velocity curves in Fig. 6. For all of the curves but the lowest-order symmetric mode, the group velocity is found to be less than the phase velocity (normal dispersion). For the lowest-order symmetric mode, however, the group velocity is greater than the phase velocity (anomalous dispersion).

The results depicted in Fig. 6 are qualitatively similar to those seen with Lamb waves. For each mode (except the lowest-order symmetric

and antisymmetric modes), there is a cutoff frequency below which the wave cannot propagate. For the lowest-order symmetric mode, the phase velocity goes asymptotically to zero as the frequency approaches zero, whereas the phase velocity of the lowest-order antisymmetric mode approaches the Rayleigh velocity. The high-frequency asymptotic limit is the fluid velocity. For Lamb waves, however, the high-frequency asymptotic limit is the Rayleigh velocity, and the low-frequency limit for the surviving mode is[11]

$$C/C_t = 2[(\kappa^2 - 1)/\kappa^2]^{1/2} ,$$

where $\kappa = C_l/C_t$.

We next searched for leaky modes, although we did not expect to find any for the case of water between SiO_2. No leaky modes were found.

In general, one would expect to find leaky modes only when the shear wave velocity in one of the solids is less than the interface wave velocity. To investigate this, we considered the case of a fluid layer between fused quartz and isotropic CdS. This structure was also studied by Wang,[12] who observed a leaky wave in the CdS. The material properties of CdS, obtained by suitably averaging the single crystal values, are $\rho = 4.82$ g/cm^3, $C_l = 4.218$ km/s, and $C_t = 1.799$ km/s.

Although the leaky wave modes are dispersive, we examined the quartz-CdS structure for a single frequency only. To properly display the results would require a three-dimensional plot, since both real and imaginary parts of the interface wave velocity will vary with frequency. The search was restricted to the region $0 < C_r < 4$ and $-0.3 < C_i < 0$. The program found two roots in the indicated range for a normalized layer half thickness of 1. The first root has not been analyzed completely and will be ignored here. The other root, which is very close to the expected position, is

$$C = 3.17343 - i\ 0.01732 \text{ km/s} .$$

This value is very close to the Rayleigh wave velocity for fused quartz. The wave vectors were

$$\alpha_0 = 3.74577 - i\ 0.00571\ \mathrm{mm}^{-1}\ ,$$

$$\alpha_1 = 1.62711 + i\ 0.01315\ \mathrm{mm}^{-1}\ ,$$

$$\beta_1 = 0.84620 + i\ 0.02528\ \mathrm{mm}^{-1}\ ,$$

$$\alpha_2 = 1.30427 + i\ 0.01640\ \mathrm{mm}^{-1}\ ,$$

$$\beta_2 = -0.00743 - i\ 2.87724\ \mathrm{mm}^{-1}\ .$$

As before, the vector β_2 indicates that the leaky wave is propagating in the CdS at an angle of 34°.5 with respect to the normal to the interface.

Since the material properties for isotropic CdS might be questionable and since the acquiring of a sample might be difficult, we repeated our calculations for a fluid layer between quartz and brass. The properties of the brass are $\rho = 8.094$ g/cm^3, $C_l = 3.83$ km/s, and $C_t = 2.05$ km/s. Again we restricted the frequency to a single value. Two roots were found in the indicated range. The faster phase velocity is given by

$$C = 3.16786 - i\ 0.00827\ \mathrm{km/s}\ .$$

Again, this value is close to the Rayleigh wave velocity of the quartz. The wave vectors are

$$\alpha_0 = 3.74389 - i\ 0.00274\ \mathrm{mm}^{-1}\ ,$$

$$\alpha_1 = 1.63139 + i\ 0.00630\ \mathrm{mm}^{-1}\ ,$$

$$\beta_1 = 0.85417 + i\ 0.01202\ \mathrm{mm}^{-1}\ ,$$

$$\alpha_2 = 1.11474 + i\ 0.00921\ \mathrm{mm}^{-1}\ ,$$

$$\beta_2 = -0.00440 - i\ 2.33671\ \mathrm{mm}^{-1}\ .$$

The leaky wave is thus propagating in the brass at an angle of 40°.3 with respect to the normal to the interface.

CASE 5: THREE-LAYER SOLID

The secular determinant for the three-layer solid is given by Eq. (20). We began by considering the case of zirconia coupons brazed with a commercial silver-based alloy. The properties of the zirconia are $\rho = 5.66$ g/cm^3, $C_l = 7.04$ km/s, and $C_t = 3.74$ km/s. Unfortunately, the material properties of the braze were not available, and the material itself was only about 75 μm thick. Since the major constituent is silver, however, we simply assumed the properties to be those of silver, which are $\rho = 10.5$ g/cm^3, $C_l = 3.6$ km/s, and $C_t = 1.59$ km/s.

We first searched for guided (undamped) waves by restricting the analysis to the real velocity axis. The search covered the range $0 < C_r < 4$ km/s. The braze layer half thickness and frequency range were chosen to yield a normalized thickness (layer half thickness divided by the wavelength of a shear wave in the braze) of $0 < h/\lambda < 2$. For a total braze layer thickness of 75 μm, the frequency at $h/\lambda = 1$ would be $\approx$42 MHz.

Figure 7 shows the dispersion curves obtained for guided waves in the zirconia joint. As in the case of the fluid layer, the permissible modes are alternating pure symmetric or antisymmetric waves. The high-frequency limit of these modes tends toward the phase velocity of a shear wave in the braze material. This is to be expected since the high-frequency limit corresponds to infinite thickness of the braze layer; hence, the result should approach a bulk wave in the braze. For each mode except the lowest-order antisymmetric one, there is a low-frequency cutoff below which the mode cannot propagate. For the lowest-order mode, however, the wave survives as the frequency (or the layer thickness) goes to zero. The limiting value of the phase velocity of this wave is just that of a shear wave in zirconia.

Although the group velocities of these modes were not calculated, the curves suggest that each mode is characterized by normal dispersion (i.e., the group velocity is less than the phase velocity and propagates in the same direction). For some material combinations, however, it is possible for the group velocity to be negative; the wave propagates backward (i.e., opposite to the phase velocity). This decidedly strange

ORNL-DWG 89-5800

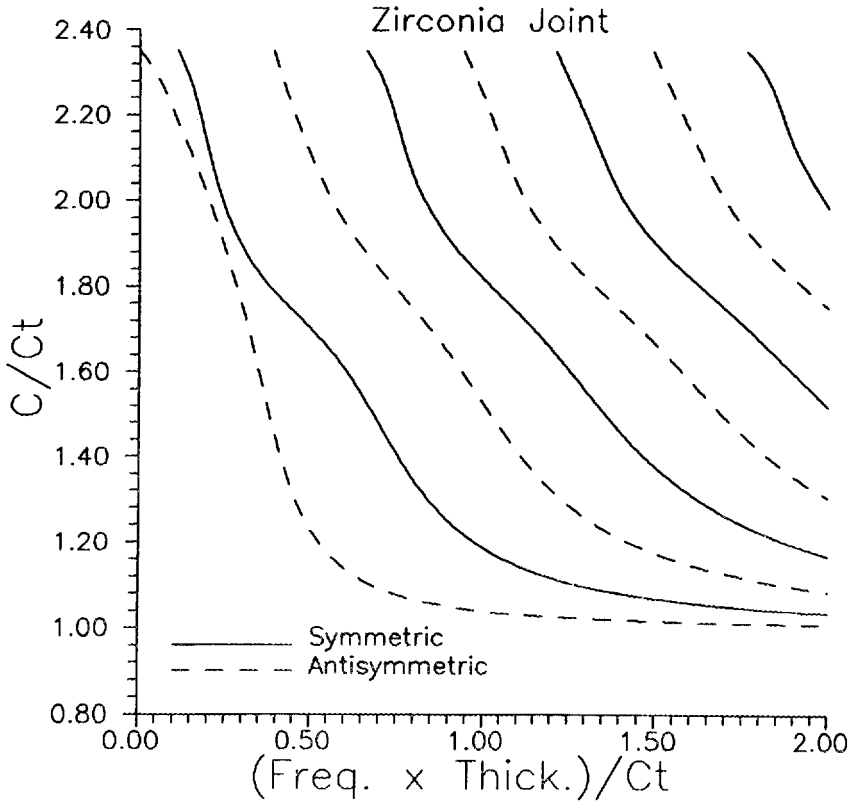

Fig. 7. Dispersion curves for guided waves in the braze layer of a zirconia joint.

behavior has just been reported for Lamb waves,[13] where backward propagating waves were theoretically predicted and experimentally observed.

Since we would expect the zero-thickness solutions of the three-layer problem to reduce to that of Stoneley waves, we next chose a material combination which is known to support such waves. We therefore chose the case of titanium bonded to iron by a thin braze layer. The existence of a Stoneley wave at a titanium-iron interface was shown earlier in this report, and this material combination also occurs in the typical ceramic transition joint. We assume that the braze layer is silver, so the material properties of all three components have been given previously. We again restrict the search for roots to the real

velocity axis in order to determine if guided waves may exist. The range for the search was $0 < C_r < 4$ as before, and the frequency range was chosen to provide a normalized thickness range of $0 < h/\lambda < 2$. Figure 8 shows the results, which are quite similar to the case of zirconia bonded to zirconia. The curves are different from the zirconia joint, however, for finite-layer thicknesses.

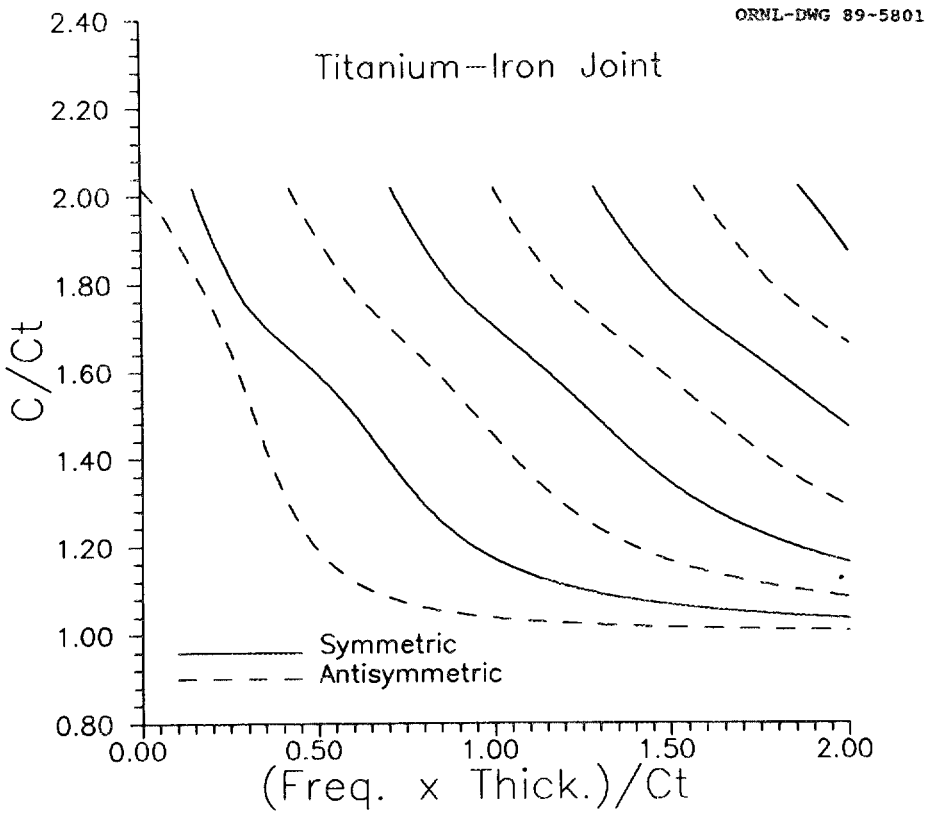

Fig. 8. Dispersion curves for guided waves in the braze layer of an iron-titanium joint.

The major difference between Figs. 7 and 8 is given by the limits of the lowest-order antisymmetric modes. For the zirconia joint, the limit is just the zirconia shear wave phase velocity. For the titanium-silver-iron joint, the limiting phase velocity approaches the value 3.20865 km/s as the thickness is reduced; thus, this wave is the

Stoneley wave found earlier for the titanium–iron structure. The wave is now dispersive, however, and is analogous to the dispersive Rayleigh wave found for the fluid layer.

By comparing Figs. 7 and 8, we can get some idea of the sensitivity of the guided–wave velocity to the properties of the ceramic adjacent to the braze layer. Recall that, for Fig. 7, the materials adjacent to the braze were zirconia whereas, for Fig. 8, they were titanium and iron. In both cases the braze material was silver. The differences in the figures may thus be attributed to changes in the bounding solids. Comparing the figures, we see that there is virtually no difference for each mode once the frequency is sufficiently high. In other words, the guided–wave velocity is insensitive to the properties of the bounding solids at high frequencies. This could be expected from the fact that, at high frequencies, the guided wave becomes indistinguishable from an ordinary shear wave in the braze layer. On the low–frequency portion of a given mode's dispersion curve, however, there are measurable differences in the results for different bounding solids. It therefore appears that, although the sensitivity to changes in the properties of the bounding solids is not particularly great, it should certainly be adequate to detect at least gross changes in the properties of the bounding solids.

We next examined the possibility of leaky waves in the braze layer of a ceramic joint. We initially chose the zirconia–silver–zirconia joint, although we did not expect any leaky modes for this structure. The search was limited to the ranges $0 < C_r < 4$ and $-0.3 < C_i < 0$. As in the case of the fluid layer, we restricted the search to a single frequency, one for which $h/\lambda = 1$. As expected, no complex roots were found.

We next searched for leaky waves in the titanium–silver–iron joint. The search range was the same as above, and the results were obtained at a single frequency. As before, no leaky waves were found within the indicated velocity range. When we examined the aluminum–silver–iron joint, however, a leaky mode was found. The analysis, which would require a three–dimensional plot for proper display and results at many more frequencies, is incomplete. However, it does appear that leaky

interface waves, in a region of practical values of attenuation, do occur in the three-layer structure.

BONDING MODEL

The *raison d'être* for the guided-wave studies was the possible establishment of a technique to assess bond strength directly for typical ceramic joints. The question of bond strength was considered by Rokhlin, Hefets, and Rosen,[14] who showed that the wave velocity of an interface wave propagating along the boundary between two solids coupled by a thin viscoelastic layer varied between the Rayleigh wave velocity and the velocity of a shear wave in the layer as the boundary conditions varied from slip contact to rigid contact. A similar result, valid regardless of the layer thickness, was obtained by Murty[15] and by Banghar and Murty.[16] In the Banghar–Murty model, which is the one we shall adopt, a viscoelastic layer having viscosity η is again inserted between the two solids whose bonding is to be modeled. Banghar and Murty[16] noted that, if one considers the parameter η/h (which they called the bonding parameter and where h is the thickness of the layer), then the secular determinant assumes three forms, depending on the limit of η/h as $h \to 0$. The limits and the bond conditions which they represent are

$\eta/h \to \infty$: Welded interface ,

$\eta/h \to 0$: Smooth interface ,

η/h = finite value: Loosely bonded interface .

In other words, as the bonding parameter increases without limit, the problem reduces to that of two solids with perfect bonding. As the bonding parameter goes to zero, the boundary condition is that of frictionless (slip) contact. For finite values of the bonding parameter, the problem becomes that of two solids which are loosely bonded.

The major result of Murty's[15] parametric study of bonding is that the interface wave velocity varies smoothly between limits as the degree of bonding increases. Working with a variable, Ψ, whose value lies in the range from 0 to 1 and which is obtained from the bonding parameter by transformation, Murty showed that, in the limit of slip contact ($\Psi \rightarrow 0$), the interface wave velocity reduces to the Rayleigh wave velocity, which is to be expected. As the bonding increases to that appropriate to welded contact ($\Psi \rightarrow 1$), the interface wave velocity increases smoothly to the Stoneley velocity, which is also reasonable. The implication of this result is that the degree of bonding can be determined by measuring the interface wave velocity.

Murty also found that, for both extremes of the bonding parameter, the interface wave velocity is pure real [i.e., the wave is a trapped (guided) wave]. At all intermediate values of Ψ, however, the wave is leaky, and thus the interface wave can be generated by mode conversion of a shear wave in the leaky medium. This result is very important for nondestructive evaluation since the phase velocity of the interface wave can be measured simply by measuring the critical angle necessary to excite the leaky wave.

For the ceramic joint problem, the model described above was applied by introducing a viscoelastic layer between the ceramic and the braze layer, thus giving two finite layers between semi-infinite half spaces. The secular determinant for this case is thus 12×12 and has been determined. Our intention is to study the effect of this layer on the previously computed modes, depicted in Figs. 7 and 8, as a function of the bonding parameter defined by Murty. This work is not yet complete.

EXPERIMENT

To confirm the results presented in Figs. 7 and 8, which are trapped modes confined to the braze layer of the ceramic joint, we designed the sample shown in Fig. 9. The ceramic materials are zirconia, and the geometry of the sample was chosen to permit surface waves to be generated on the larger of the two coupons (which would then

YP-4625

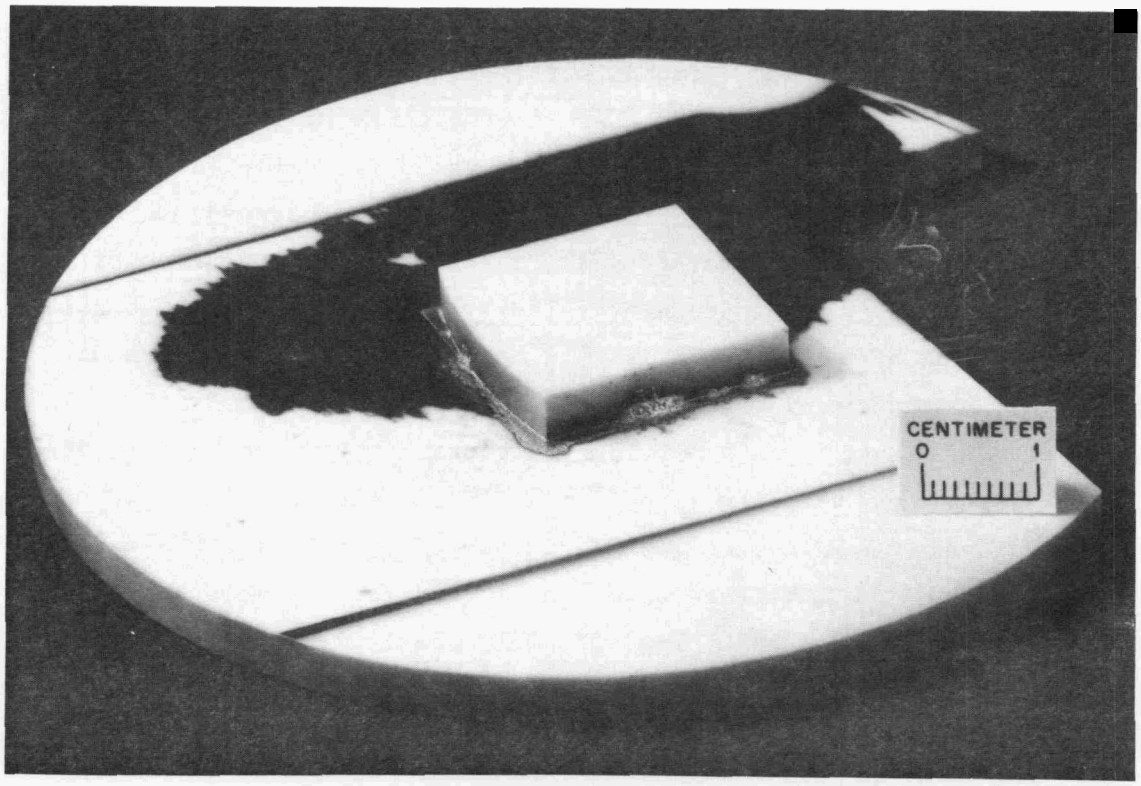

Fig. 9. Zirconia joint sample for interface wave studies.

excite guided waves in the braze layer) and be detected by a similar surface wave transducer on the other side of the joint. Before any attempt to excite surface waves, however, the braze layer was first interrogated with high-frequency compressional waves focused at the interface in order to determine whether gross nonbonds were present. The results are shown in Fig. 10, where the dark regions are essentially completely nonbonded. The sample was thus totally unsuitable. Destructive analysis of the joint indicated that the problem was due to extreme porosity in the braze layer.

Several additional samples of similar design were also procured. All were found to have similar problems of porosity, and one coupon was severely cracked as well. These results are not typical of the joints

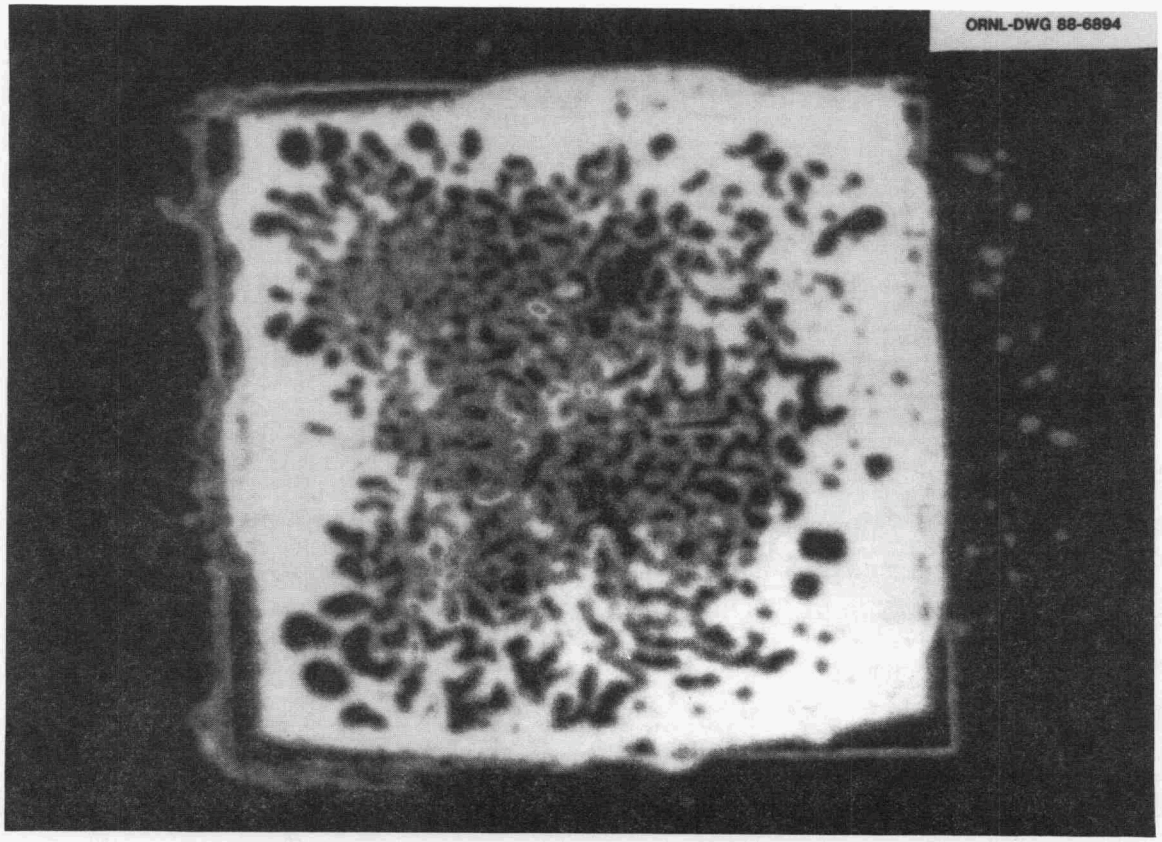

Fig. 10. Ultrasonic scan of braze joint region.

previously produced on this program. Since no suitable specimens were obtained, we were unable to verify experimentally the theoretical predictions.

SUMMARY AND CONCLUSIONS

The theory of guided elastic waves propagating in the braze layer of a ceramic joint was developed. The secular determinant for this case was obtained, and a FORTRAN program was written to find the roots of the secular equation. A number of cases were treated numerically, and both guided and leaky waves were found for various choices of materials bonded with a thin layer of silver. In the case of identical solids bonded by a thin layer, no interface waves were found in the limit of

vanishing layer thickness, and no leaky waves were found for any value of layer thickness. For different solids known to have a Stoneley wave at the welded interface, a dispersive Stoneley wave was found. A possible bonding model was examined by introducing a thin viscoelastic layer between one of the bonding solids and the braze layer. The secular determinant was obtained for this case, but the analysis is not complete. Several joint specimens were obtained for experimental analysis, but none of these samples was suitable for interface wave studies.

From this study, it appears that elastic guided waves will be of considerable benefit to the evaluation of the state of bonding in typical ceramic joints. Additional theoretical work should be performed to establish the sensitivity of this technique to small changes in the conditions occurring at the braze-ceramic interface, and further development of the root-seeking algorithms would be advantageous. Since there is now strong theoretical evidence to support the contention that the typical ceramic joint can indeed support guided waves and the behavior of these waves is indicative of the state of bonding at the braze-ceramic interface, additional samples should be fabricated which exhibit varying degrees of bonding for experimental confirmation. Additional wave types, such as horizontally polarized guided waves, should also be studied, since the polarization of the interrogating radiation is often quite important in many problems in nondestructive evaluation.

ACKNOWLEDGMENTS

The authors would like to express their thanks to M. L. Santella and L. C. Emerson of the Materials Joining group for their help in the fabrication of the samples used in this study. They would also like to thank T. D. K. Ngoc of Georgetown University for many helpful suggestions and discussions during the theoretical development and for pointing out the bonding model of Banghar and Murty.

REFERENCES

1. W. A. Simpson and R. W. McClung, *Ultrasonic Techniques for the Evaluation of Ceramic Joints*, ORNL-6350, April 1987.

2. Lord Rayleigh, "On Waves Propagated Along the Plane Surface of an Elastic Solid," *Sci. Pap.* **II**, 441 (1886).

3. Horace Lamb, "On Waves in an Elastic Plate," *Proc. R. Soc. London, Ser. A* **93**, 114–28 (1917).

4. A. E. H. Love, *Some Problems of Geodynamics*, Cambridge University Press, London, 1911, 1926.

5. R. Stoneley, "Elastic Waves at the Surface of Separation of Two Solids," *Proc. R. Soc. London, Ser. A* **106**, 416–28 (1924).

6. R. Truell, C. Elbaum, and B. B. Chick, *Ultrasonic Methods in Solid State Physics*, Academic Press, New York, 1969.

7. *Standard Mathematical Tables, Sixteenth Edition*, The Chemical Rubber Company, Cleveland, 1968.

8. P. W. Staecker and W. C. Wang, "Propagation of Elastic Waves Bound to a Fluid Layer Between Two Solids," *J. Acoust. Soc. Am.* **53**(1), 65–74 (1973).

9. W. Pilant, "Complex Roots of the Stoneley Wave Equation," *Bull. Seismol. Soc. Am.* **62**, 285 (1972).

10. D. A. Lee and D. M. Corbly, "Use of Interface Waves for Nondestructive Testing," *IEEE Trans. Sonics Ultrason.* **SU-24**, 206–12 (1977).

11. J. D. Achenbach, *Wave Propagation in Elastic Solids*, North-Holland, Amsterdam, 1980.

12. W. C. Wang, "Propagation and Amplification of Ultrasonic Waves in a Layered Structure of Quartz-Liquid-CdS," *J. Appl. Phys.* **41**(1), 1–3 (1970).

13. J. Wolf, T. D. K. Ngoc, R. Kille, and W. G. Mayer, "Investigation of Lamb Waves Having a Negative Group Velocity," *J. Acoust. Soc. Am.* **83**, 122–32 (1988).

14. S. Rokhlin, M. Hefets, and M. Rosen, "An Elastic Interface Wave Guided by a Thin Film Between Two Solids," *J. Acoust. Soc. Am.* **51**(7), 3579–82 (1980).

15. G. S. Murty, "A Theoretical Model for the Attenuation and Dispersion of Stoneley Waves at the Loosely Bonded Interface of Elastic Half Spaces," *Phys. Earth Planet. Inter.* **11**, 65–79 (1975).

16. A. R. Banghar and G. S. Murty, "On the Parametric Model of Loose Bonding of Elastic Half Spaces," *J. Acoust. Soc. Am.* **60**(5), 1071–77 (1976).

INTERNAL DISTRIBUTION

1-2. Central Research Library
3. Document Reference Section
4-5. Laboratory Records Department
6. Laboratory Records, ORNL RC
7. ORNL Patent Section
8-10. M&C Records Office
11. P. Angelini
12. R. L. Beatty
13. P. F. Becher
14. T. M. Besmann
15. R. A. Bradley
16. C. R. Brinkman
17. R. S. Carlsmith
18. D. F. Craig
19. M. G. Jenkins
20. K. C. Liu
21-25. R. W. McClung
26. D. J. McGuire
27. A. J. Moorhead
28. M. E. O'Hern
29. M. L. Santella
30. A. C. Schaffhauser
31. B. W. Sheldon
32-36. W. A. Simpson, Jr.
37. G. M. Slaughter
38. D. P. Stinton
39. J. R. Weir
40. A. D. Brailsford (Consultant)
41. H. D. Brody (Consultant)
42. F. F. Lange (Consultant)
43. D. P. Pope (Consultant)
44. E. R. Thompson (Consultant)
45. J. B. Wachtman, Jr. (Consultant)

EXTERNAL DISTRIBUTION

46. Kamal Amin, Norton Company, High Performance Ceramics, Goddard Road, Northboro, MA 01532-1545

47. D. I. Biehler, Caterpillar, Inc., Technical Center, P.O. Box 1875, Peoria, IL 61656-1875

48. Les Bowen, GTE Laboratories, Inc., 40 Sylvan Road, Waltham, MA 02254

49. Steve Bradley, Signal UOP Research Center, 50 UOP Plaza, Des Plaines, IL 60016-6187

50. Annette Comfort, Garrett Auxiliary Power Division, Dept. 93-172, Mail Stop 1303-2, 2739 East Washington Street, P.O. Box 5227, Phoenix, AZ 85010

51. N. D. Corbin, Advanced Ceramics, Norton Co., Goddard Road, Northboro, MA 01532-1545

52. Ben Cross, Southwest Research Institute, P.O. Drawer 28510, San Antonio, TX 78284

53. R. A. Cutler, Ceramatec, Inc., 2425 South 900 West, Salt Lake City, UT 84119

54. K. F. Dufrane, Battelle Columbus Laboratories, 505 King Avenue, Columbus, OH 43201-2693

55. J. J. Eberhardt, Department of Energy, ECUT Division, 1000 Independence Avenue, SW, Washington, DC 20585

56. W. A. Ellingson, Materials Science and Technology Division, Argonne National Laboratory, 9700 South Cass Avenue, Argonne, IL 60439

57. Dana Elliott, Los Alamos National Laboratory, P.O. Box 1663, Los Alamos, NM 87545

58. R. C. Evans, Assistant Manager, Vehicular Gas Turbine and Diesel Project Office, NASA Lewis Research Center, 21000 Brookpark Road, MS-77-6, Cleveland, OH 44135

59. John Fairbanks, Office of Transportation Systems, Propulsion Division, Department of Energy, Forrestal Building, 1000 Independence Avenue SW, Washington, DC 20585

60. D. M. Forney, Air Force Wright Aeronautical Laboratory, AFWAL/WRDC, Wright-Patterson AFB, OH 45433

61. William Friedman, British Petroleum Company, Warrensville Center Road, Cleveland, OH 44128

62. G. E. Gazza, Ceramics Research Division, U.S. Army Materials Technology Laboratory, 405 Arsenal Street, Watertown, MA 02172-0001

63. R. E. Green, Jr., The Johns Hopkins University, Center for Nondestructive Evaluation, Baltimore, MD 21218

64. Nabil Hakiem, General Motors Corporation, Allison Gas Turbine Operations, P.O. Box 420, Indianapolis, IN 46206-0420

65. N. L. Hecht, University of Dayton Research Institute, 300 College Park, Dayton, OH 45469-0001

66. C. A. Johnson, General Electric Co., P.O. Box 8, K1/3C7, Schenectady, NY 12301

67. Keith Karasek, Allied-Signal Engineered Materials Research Center, East Algonquin Road, Box 5016, Des Plaines, IL 60017-5016

68. R. N. Katz, U.S. Army Materials Technology Laboratory, 405 Arsenal Street, Watertown, MA 02172-0001

69. Promod Khanderwahl, General Motors Corporation, Allison Gas Turbine Operations, P.O. Box 420, Indianapolis, IN 46206-0420

70. H. J. Kim, GTE Laboratories, Inc., 40 Sylvan Road, Waltham, MA 02254

71. S. J. Klima, NASA Lewis Research Center, 21000 Brookpark Road, Cleveland, OH 44135,

72. S. B. Kramer, Department of Energy, Forrestal Building CE-151, 1000 Independence Avenue SW, Washington, DC 20585

73. A. S. Krieger, President, Radiation Science, Inc., P.O. Box 293, Belmont, MA 02178

74. S. R. Levine, NASA Lewis Research Center, 49-3, 21000 Brookpark Road, Cleveland, OH 44135

75. Laymon Lott, EG&G, Inc., Idaho National Engineering Laboratory, P.O. Box 1625, Idaho Falls, ID 83415

76. Janet Minter, Southwest Research Institute, P.O. Drawer 28510, San Antonio, TX 78284

77. J. N. Panzarino, Norton Company, High Performance Ceramics, Goddard Road, Northboro, MA 01532-1545

78. A. E. Pasto, GTE Laboratories, Inc., 40 Sylvan Road, Waltham, MA 02254

79. J. W. Patten, Director, Materials Engineering, Cummins Engine Company, Box 3005, Mail Code 50183, Columbus, IN 47202-3005

80. Vickie Paubuise, Garrett Auxiliary Power Division, P.O. Box 5227, Phoenix, AZ 85010

81. Thomas Powers, Babcock and Wilcox, Old Forrest Road, Lynchburg, VA 24505

82. Peter Purdue, Detroit Diesel Corporation, 13400 Outer Drive, Detroit, MI 48239-4001

83. D. W. Richerson, Ceramatec, Inc., 2425 South 900 West, Salt Lake City, UT 84119

84. S. L. Richlen, U.S. Department of Energy, Office of Industrial Programs, Forrestal Building, CE-141, 1000 Independence Avenue, Washington, DC 20585

85. G. A. Rossi, Advanced Ceramics, Norton Co., Goddard Road, Northboro, MA 01532-1545

86. J. S. Salem, NASA Lewis Research Center, 21000 Brookpark Road, Cleveland, OH 44135

87. J. Sankar, Department of Mechanical Engineering, North Carolina A&T State University, Greensboro, NC 27411

88. Maxine Savitz, Director, Garrett Ceramic Components Division, Allied-Signal Aerospace Company, 19800 S. Van Ness Avenue, Torrance, CA 90509

89. R. B. Schulz, Department of Energy, Forrestal Building, 1000 Independence Avenue SW, Washington, DC 20585

90. James Seydel, EG&G, Inc., Idaho National Engineering Laboratory, P.O. Box 1625, Idaho Falls, ID 83415

91. Jay Smyth, Garrett Auxiliary Power Division, Allied-Signal Aerospace Company, 2739 East Washington Street, Phoenix AZ 85010

92. Roger Storm, Carborundum Co., P.O. Box 1054, Niagara Falls, NY 14302

93. D. O. Thompson, Iowa State University, Ames Laboratory, Ames, IA 50011

94. C. D. Weiss, Caterpillar, Inc., 100 N.E. Adams Street, Peoria, IL 61629

95. D. E. Wittmer, Department of Mechanical Engineering and Energy Processes, Southern Illinois University, Carbondale, IL 62901

96. Alex Vary, NASA Lewis Research Center, 21000 Brookpark Road, Cleveland, OH 44135

97. S. K. Vin, GTE Laboratories, Inc., 40 Sylvan Road, Waltham, MA 02254

98. Thomas Yolkan, National Institute of Standards and Technology, Gaithersburg, MD 20899

99. T. M. Yonuschonis, Cummins Engine Company, Box 3005, Mail Code 50183, Columbus, IN 47202-3005

100. Donald Yuhas, Allied Signal Research Center, 50 UOP Plaza, Des Plaines, IL 60016

101. Assistant Manager for Energy Research and Development, Department of Energy, Oak Ridge Operations Office, P.O. Box 2001, Oak Ridge, TN 37831-8600

102-111. Department of Energy, Office of Scientific and Technical Information, Office of Information Services, P.O. Box 62, Oak Ridge, TN 37831

For distribution by microfiche as shown in DOE/OSTI-4500, Distribution Category UC-365 (High-Temperature Materials).

☆U.S. GOVERNMENT PRINTING OFFICE 1989—748-114/00086